



Ultrathin, elastic, and self-adhesive nanofiber bio-tape: An intraoperative drug-loading module for ureteral stents with localized and controlled drug delivery properties for customized therapy[☆]

Liheng Gao^a, Mingxi Xu^b, Wenshuo Zhao^a, Ting Zou^a, Fujun Wang^a, Jun Da^{b,***}, Yiwei Wang^{b,**}, Lu Wang^{a,*}

^a Key Laboratory of Textile Science and Technology, Ministry of Education, College of Textiles, Donghua University, Shanghai, 201620, China

^b Department of Urology, Ninth People's Hospital, School of Medicine, Shanghai Jiaotong University, Shanghai, 200011, China

ARTICLE INFO

Keywords:

Intraoperative drug delivery
Customized therapy
Ureteral stent
Urinary tract infection

ABSTRACT

During the postoperative management of urinary diseases, oral or intravenous administration of drugs and implanting ureteral stents are usually required, making localized drug delivery by ureteral stent a precise and effective medication strategy. In the traditional drug loading method, the drug was premixed in the implants in production lines and the versatility of drugs was restricted. However, the complex situation in the urinary system fails the possibility of finding a “one fits all” medication plan, and the intraoperative drug-loading of implants is highly desired to support customized therapy. Here, we designed an ultrathin (8 μm), elastic, and self-adhesive nanofiber bio-tape (NFBT) that can easily encapsulate drugs on the stent surface for controllable localized drug delivery. The NFBT exhibited high binding strength to a ureteral stent, a sustained release over 7 d in PBS for hydrophilic drug, and a zero-order release curve over 28 days for the hydrophobic drug nitrofurantoin (NFT). Further *in vivo* experiments using a porcine ureteral tract infection model demonstrated that NFBT loaded with NFT could significantly reduce the bacterial concentration in urine. The total amount of NFT delivered by the NFBT was about 2.68 wt% of the recommended dose for the systemic administration.

1. Introduction

Oral or intravenous administration of drugs is usually required postoperatively for patients with urinary diseases such as calculi, ureteral neoplasms, and strictures. Drugs must pass through the whole body where they may be metabolized before concentrating and functioning in the urine. Thus the drug utilization rate is low. For example, nitrofurantoin (NFT), a common oral administered antibiotic for urinary tract infection (UTI), can excrete into the urine for merely 30–40%. Furthermore, in renal failure cases, the kidneys may not be able to excrete an effective concentration of medicine into the urine. Let alone systemic side effects induced by excessive accumulation of drugs in the blood. As a result, in renal insufficiency cases, dosage reduction is required for many kinds of medicines such as Levofloxacin, another

commonly used antibiotic for UTIs. Moreover, urinary tract obstruction may still further reduce the concentration of antimicrobial agents within the urine [1–3].

In this regard, localized administration is an appropriate alternative treatment strategy, because it can maintain the original molecular structure of medicines, permitting the direct and precise use of target drugs as well as expanding the range available [4–7]. In the lower urinary tract, localized drug delivery can be achieved by irrigation of the medicine into the bladder via a urethral catheter [8–10]. However, this method is not suitable for the treatment of upper urinary tract diseases. On the other hand, postoperative ureteral stent (US) placement is widely used for many urinary system disorders. Clinically used USs are soft hollow tubes with double-J ends. Its upper end is usually placed in the renal pelvis and the lower end in the bladder giving the stents access to

[☆] Liheng Gao and Mingxi Xu contributed equally to this work. Peer review under responsibility of KeAi Communications Co., Ltd.

* Corresponding author. Key Laboratory of Textile Science and Technology, Ministry of Education, College of Textiles, Donghua University, Shanghai, 201620, China.

** Corresponding author. Department of Urology, Ninth People's Hospital, School of Medicine, Shanghai Jiaotong University, Shanghai, 200011, China.

*** Corresponding author. Department of Urology, Ninth People's Hospital, School of Medicine, Shanghai Jiaotong University, Shanghai, 200011, China.

E-mail addresses: phillda@sh9hospital.org (J. Da), wang_yiwei@yeah.net (Y. Wang), wanglu@dhu.edu.cn (L. Wang).

<https://doi.org/10.1016/j.bioactmat.2022.03.025>

Received 3 November 2021; Received in revised form 14 February 2022; Accepted 15 March 2022

Available online 22 March 2022

2452-199X/© 2022 The Authors. Publishing services by Elsevier B.V. on behalf of KeAi Communications Co. Ltd. This is an open access article under the CC BY-NC-ND license (<http://creativecommons.org/licenses/by-nc-nd/4.0/>).

both the lower and upper urinary tract as well as the partial pelvis. Clinically, the possibility of constructing a long-term controllable drug delivery and release system within the US is a relatively simple concept for postoperative urinary system treatments.

Except for the requirement of localized administration, the complex and various situation in the urinary system fails the possibility of finding a “one fits all” medication plan. For example, the bacterial susceptibility varies dramatically in patients exposed to antimicrobial agents and in individuals in inpatient and outpatient settings. Each clinician must keep abreast of changes that affect antimicrobial use and susceptibility patterns. Therefore, customized therapy is regarded with a clinical prospect, and surgeons can decide the type and dose of the drug in the middle of operation according to the observed surgical fields and specific clinical indications. The loading of drugs should be carried out intraoperatively, which means after polymer molding and before implantation of the US.

Nevertheless, the present drug delivery systems are unable to simultaneously comply with the requirement of localized and customized therapy in the urinary tract. The traditional approach is to encapsulate drugs in a polymer by co-diffusing the two materials in an organic solvent, and the drugs are then trapped in the matrix following removal of the solvent [11]. During the release process, drugs can be slowly dissolved in the aqueous solution of the polymer interspace or as the matrix degrades [12,13]. Among these polymers, hydrogel is one of the most typical drug-loading materials. However, it is incompatible with hydrophobic drugs because of the loose structure and hydrophilic nature of hydrogel [14–19]. In addition, the adhesion strength of the hydrogel to the US is also weakened by its swelling features [20–22]. Other preparation techniques for drug carriers include 3-D printing [23–26], solvent casting [27], and micro-nano capsules [28–31]. However, the drug-loading process (type, dose) is usually carried out before polymer molding and cannot be adjusted in use.

The flexible drug loading strategy calls for a compatible loading and releasing system. Due to large differences in the chemical properties of drugs and the complexities of surgical operations, chemical methods can be excluded. Meanwhile, the wide-used physical methods including a simple dipping or blending method are also unsuitable in this situation, because the ureteral system is a fluid environment, controlled drug release is difficult to realize especially by simple physical adsorption. Therefore, an encapsulation strategy, i.e., the design of a nanoporous membrane to encapsulate a drug to the stent surface, may be a solution to control drug release [32–34]. The precondition for the strategy is that the membrane possesses adequate adhesive properties towards the stent surface to ensure good sealing performance. Interestingly, electrospun nanofiber membranes, which possess numerous nanopores generated by interlaced nanofibers, meet these requirements. The electrostatic force generated by the electret of electrospun nanofibers endows the materials with adhesion performance. To further improve the adhesion effect, the membrane should also possess a certain elasticity to reinforce the radial pressure on the stent.

In this study, an elastic, self-adhesive, and ultrathin nanofiber biotape (NFBT) was developed by electrospinning biocompatible polycaprolactone (PCL). The pre-wetted bio-tape was then coated with solid drug powders and rolled onto the US under tension. As a result, a multilayered stent-drug-nanofiber membrane structure was constructed. Urinary tract infection (UTI) is a common disease in the urinary system that is usually induced by the implantation of a ureteral stent, and antibiotics should be carefully selected according to the antimicrobial spectrum. Herein, the white porcine UTI model was used to evaluate the in vivo drug releasement and treatment effect of NFBT. The following characteristics were determined: (i) binding strength to the ureteral stent; (ii) release of both hydrophilic and hydrophobic drugs; (iii) biocompatibility; and (iv) effective dose.

2. Experimental section

2.1. Materials

Unless otherwise indicated, all chemicals were purchased from Sinopharm Chemical Reagents Co. (Shanghai, China) and used as received.

2.2. Fabrication and drug loading method of NFBT

The NFBTs were fabricated using a TL-Pro electrospinning machine (Tong Li Weina Technology Co., Ltd., Shenzhen, Guangdong, China) using a 20-gauge blunt steel needle. PCL was dissolved in dichloromethane/dimethylformamide (7/3 v/v) with vigorous magnetic stirring to obtain a clear solution with a concentration of 12.5% (w/v). Spinning was carried out at a flow rate of 1 mL/h, applied voltage of 20 kV, and a collecting distance of 20 cm. During the spinning process, SH powder (total amount 10 mg) was periodically sprayed onto the surface of the nanofiber membrane (five applications at 2 min intervals) to construct a multi-layer sandwich-like structure. This nanofiber membrane was named NFBT. The prepared NFBT was then placed in a vacuum oven at 37 °C for 24 h to remove the residual solvent. For the drug-loading process, the NFBT was cut into 4 cm × 8 cm sections and rehydrated with deionized water (30 µL). 150 mg of NFT or rhodamine B (RB) powder was sprayed onto the surface of NFBT (4 cm × 8 cm) using a medicine spoon. The powder was fixed on the top surface of the NFBT under the electrostatic force generated from the electrospinning process. Thereafter, the NFBT was wrapped onto the US at a predetermined tension. The predetermined tension was 0.2–0.5 N and the elongation rate of NFBT was less than 10% (Fig. S1). Ureteral stents loaded with NFBT and NFT or RB drugs were named NFBT-NFT or NFBT-RB, and ureteral stents loaded with pure NFBT were named NFBT-CTL.

2.3. Characterization of the NFBT and NFBT loaded USs

The surface morphology of the samples was observed using an S-4800 scanning electron microscope (SEM; Hitachi, Japan). The tensile properties of NFBT and its binding strength to the stents were measured using a YG (B) 026G-500 universal testing system (Wenzhou Darong Textile Instrument Co., Ltd., Wenzhou, Zhejiang, China); the elongation rate was 300 mm/min, and the gauge length was 50 mm. For binding strength, a polyurethane bar with a diameter of 2 mm was used to simulate the USs. The contact length between the polyurethane bar and NFBT was 50 mm, and the stent end and NFBT end was fixed in the chucks and moved at a speed of 300 mm/min. Three specimens were tested for each determination.

2.4. Drug release tests

The drug release characteristics of NFBT-NFT or NFBT-RB were measured in phosphate-buffered saline (PBS; 50 mL of 0.1 M, pH 6.8) to simulate drug release in vivo. Samples were placed in centrifuge tubes with the release medium at 37 °C on a mechanical shaker (60 rpm). Aliquots were periodically collected and refreshed at each time point and the absorption maxima were recorded at 375 nm (NFT) or 554 nm (RB) with a TU-1901 UV-vis spectrophotometer (Beijing Purkinje General Instrument Co., Ltd., Beijing, China).

2.5. Cytotoxicity tests

Cytotoxicity tests were conducted according to ISO10993-5-2009. Extracts were obtained by rinsing samples with PBS solution three times followed by impregnation with Dulbecco's modified Eagle's medium (DMEM; Gibco, USA) for 24 h, the extraction condition of samples was set as 6 cm²/mL, 37 °C. DMEM was mixed with 5% dimethyl sulfoxide and pure DMEM solutions were set as the positive and negative

control groups. L929 cells (The Cell Bank of Type Culture Collection of Chinese Academy of Science, Shanghai, China) were seeded in a 96-well plate at a density of 3000 cells/mL and placed in a 5% CO₂ incubator at 37 °C for 24 h. Solutions corresponding to the groups (100 µL) were added to each well and the medium was changed every 24 h. On days one and three, the morphology of cells was examined by microscopy, and the viability of L929 was determined by the Cell Counting Kit-8 (CCK-8) assay (Sangon Biotech Co., Ltd., Shanghai, China).

2.6. In vivo experiments

2.6.1. Sample preparation and implantation procedure

All animal experiments were conducted by an authorized company (Gateway Medical Innovation Center, Shanghai, China) under the animal welfare requirements of ISO 10993–2:2006 after being approved by the company's ethical committee (approval number: SH2020-10002). NFBT-CTL and NFBT-NFT were prepared as described and sterilized with ethylene oxide. Bacteria suspension was prepared by culturing *Escherichia coli* (*E. coli*, ATCC 25922) in LB medium at 37 °C overnight and adjusting to $1-2 \times 10^6$ CFU/mL with PBS (0.1 M, pH 7.0). Six female farm pigs (30–33.5 kg) were randomly divided into NFBT-US and NFBT-NFT-US groups. On the first day, bacterial suspension (10 mL) was injected into the bladder of each animal through a catheter before NFBT-US or NFBT-NFT-US groups were implanted with the stents in the left ureter of the animal using flexible ureteroscopy (Innovation, China, 8.7 F, 65 cm, disposable, digital). All animal experiments were conducted under general anesthesia.

2.6.2. Urine and blood examination

Urine was extracted from the bladder of the animals using a medical syringe after 4 h, 24 h, 4 d, 7 d, 14 d, 21 d, and 28 d of implantation. The extracted urine (1 mL) was then serially diluted for agar plating (LB agar), and the number of CFU was enumerated after 24 h.

To determine the NFT concentration in urine, an aliquot of the extracted urine (1 mL) was mixed with acetonitrile (1.8 mL) and deionized water (1.2 mL), vortex mixed for 30 s, and then sonicated (130 W/50 Hz) for 15 min. The mixture was pumped through an N-propyl ethylene diamine (PSA) solid-phase extraction cartridge (Carb-GCB/PSA, Hosea, China) before determination using a Chromaster HPLC system with UV detection (Hitachi, Japan). Samples were separated and identified under the following conditions: Injection volume, 20 µL; mobile phase, acetonitrile-water (3:2) at a flow rate of 1.0 mL/min; column, C18 (250 mm × 4.6 mm × 4.6 µm) maintained at 40 °C; detection wavelength, 365 nm.

On days 0, 1, 4, 7, 14, 21, and 28 post implantations, the serum concentrations of total bile acid (TBA), total bilirubin levels, aspartate aminotransferase (AST), and alanine aminotransferase (ALT) were measured carried out using a BS 280 automatic blood biochemical analyzer (Mindray, Shenzhen, China). Hematological tests were completed on blood samples using a BC-30 Auto Hematology Analyzer (Mindray, Shenzhen, China), and the markers (red blood cell count (RBC), white blood cell count (WBC), hemoglobin (HGB), red blood cell-specific volume (HCT), Lymphocytes (LYM)) determined.

2.6.3. Determination of biofilm and encrustations

On day 28, the stents were explanted and maintained in saline at 4 °C for subsequent characterization. For quantitative bacterial analysis, three 1 cm sections of US or NFBT were cut from the upper, middle, and lower regions and sonicated (130 W/50 Hz) in PBS solution (1 mL) for 15 min. The suspension was harvested, vortex mixed, and serially diluted for agar plate count. Meanwhile, the US or NFBT samples were fixed with paraformaldehyde (4%), stored at 4 °C for 12 h, rinsed with deionized water three times, gradient dehydrated with ethanol (10 min in 30%, 10 min in 50%, 10 min in 70%, 10 min in 90%, and 20 min in 100%), air-dried for 1 h and then sputter-coated with gold for SEM observation. A Zeiss Gemini 300 field-emission SEM (FESEM; Carl Zeiss

AG, Jenna, Germany) equipped with an X-Max 80 energy dispersive X-ray spectroscopy (EDS) attachment (Oxford Instruments, Abingdon, UK) was employed to analyze the biofilm and encrustations on the USs and NFBT; the accelerating voltage was 15 kV.

2.6.4. General observation and histological evaluation

On day 28, the pigs were euthanized, the kidney, renal pelvis, ureter, and bladder were excised and the extent of ureteral obstruction and degree of water accumulation in the kidneys was determined. The harvested specimens were then fixed in 4% paraformaldehyde, decalcified in ethylenediaminetetraacetic acid (Gibco, USA), dehydrated with ethanol, embedded in paraffin, stained with hematoxylin-eosin (HE; Gibco, USA), CD3 antibodies, CD68 monoclonal antibodies (Thermo Fisher, USA); an X71 biomicroscope (Olympus, Tokyo, Japan) was used for all histopathological observations.

2.7. Statistical analysis

Values given in figures are mean ± standard deviation and all data was checked for normality. Differences between groups were evaluated by one-way analysis of variance. The levels of statistical significance were denoted by (***) for $p < 0.001$, (**) for $p < 0.01$, and (*) $p < 0.05$.

3. Results and discussion

3.1. Morphology and mechanical behavior

The NFBT was prepared by electrospinning with SH to fill the inter-fiber space. SH is a main component of glycosaminoglycan protective layer that exist in the mucosa of the urinary system to defends tissues against irritants in urine. As a hydrophilic component, SH can also improve the hydrophilicity of NFBT, turning it from hydrophobic to hydrophilic (Fig. S2). The addition of SH can reduce the friction between implant and urethral tissue and improve biocompatibility. Fig. 1(B) and (C) show the SEM images of NFBT before and after wetting. Before wetting, powdered SH was observed. This was absent in the SEM image of hydrated NFBT, due to the high water solubility of SH. One of the main features of NFBT was its adhesive behavior and the strong bonding affinity to polyurethane (PU) material. Fig. 1(E) and (G) show that NFBT remained attached to the surface of the PU tube, i.e., it did not unwind after the tension was removed due to the van der Waals forces and friction. This self-adhesive behavior enables NFBT to remain firmly wrapped under the shear forces due to the peristaltic action of the ureter during and after implantation. Another important aspect concerns the binding integrity between NFBT and the US, which should be sufficient to prevent the displacement of the drug delivery module. To evaluate this quantitatively, the tensile strength (TS) of NFBT and the binding of NFBT to the PU tube were measured on a tensile test instrument. Fig. 1(D) and (E) show the stress-strain curves for NFBT in the dry (maximum TS, 6.81 ± 0.73 Mpa) and wet states (maximum TS, 3.69 ± 0.59 Mpa). For the tensile test (binding strength), the contact length of NFBT was set to 5 cm, the end of the test material was firmly clamped; the intentional end-point was the slippage or fracture of NFBT on the PU tube. Post testing, NFBT maintained a contact length of 5 cm, with no slippage between the PU tube and NFBT, indicating that the interaction between the stent and the membrane was greater than the breaking strength of the membrane. As a result, the stress-strain curve (Fig. 1(F)) demonstrated a similar profile to the tensile test result of NFBT, while with the enhanced elongation rate and tensile stress in the dry state due to the friction induced by the denser fibers. Compared with pure PCL membrane, the tensile behavior of NFBT in wet state declined (Fig. S3), as the addition of SH reduced the friction between nanofibers. However, no slippage was found between the PU tube and NFBT. The adhesive behavior of NFBT could be attributed to two characteristics of the materials: The electrostatic force generated by the electret of the electrospun nanofiber process (20 kV); and the inherent elasticity of NFBT,

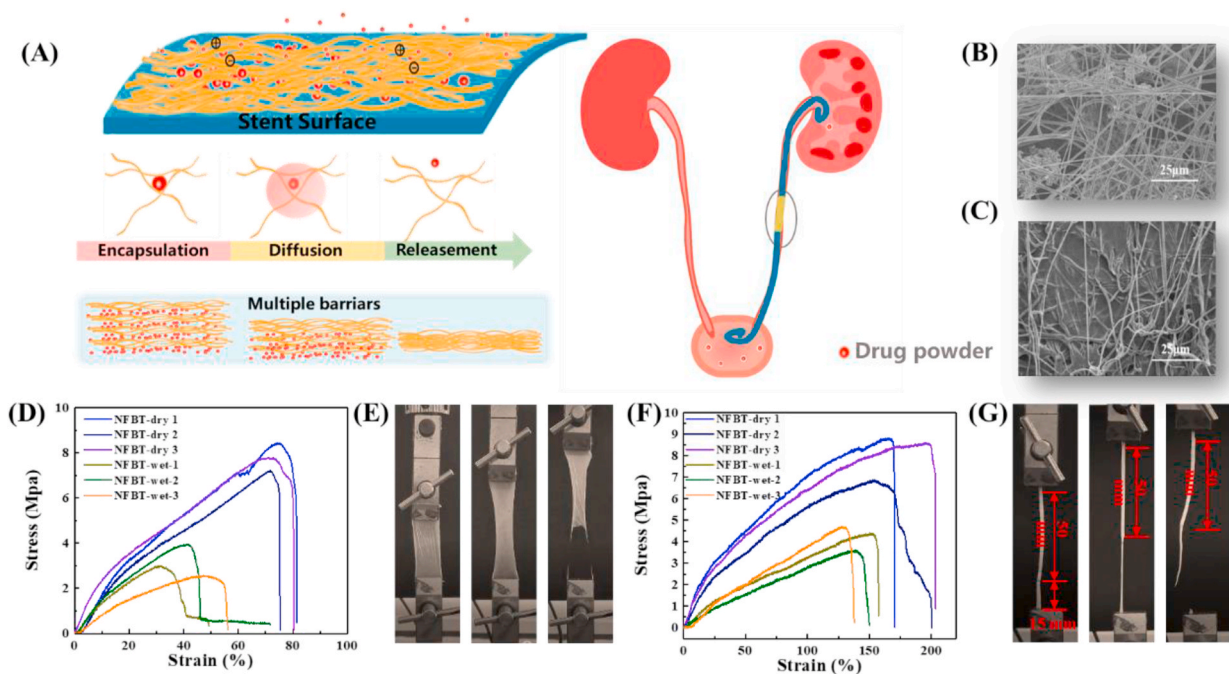


Fig. 1. Morphology and mechanical behavior of the NFBT: (A) Schematic illustration of loading strategy for NFBT and US; (B) SEM image of NFBT before wetting; (C) SEM image of NFBT after wetting; (D) stress-strain curve of NFBT; (E) behavior of NFBT during the tensile test; (F) stress-strain curve of NFBT attached to the US; and (G) behavior of NFBT during the binding strength test.

which can convert the tension into radial pressure, thereby reinforcing the friction between the NFBT and the stent.

3.2. In vitro release study of NFBT

NFT is one of the most used antibiotics for the treatment of urinary tract infections. Following oral administration, only 30–40% of the drug reaches the urinary tract, while the remainder is mainly absorbed by the intestinal tissue, often arousing intestinal discomfort. NFT is a typical lipophilic drug while rhodamine B was chosen as a water-soluble model drug. The total loading amounts of NFT and RB were 150 mg each. NFBT-NFT exhibited a constant drug release over 28 days consistent with zero-order drug release kinetics ($M_t/M_\infty = 1.04236t$, $R^2 = 0.9929$; Fig. 2(A) and (B)). Initial drug release was 0.02–0.03 mg/h in the first 24 h and was maintained at approximately 0.01 mg/h thereafter. 82.8 ± 1.75 wt% of the loaded drug was released in 28 days. The corresponding changes in the appearance and color of NFBT-NFT are shown in Fig. 2(C). To further understand the drug-release behavior, SEM images obtained from sample cross-sections showed that the even distribution of crystalline NFT powder between the layers of NFBT was maintained after 72 h of drug release (Fig. 2(D)). Since NFT was slightly soluble in water, it was difficult for water molecules to infiltrate the drug-delivery system. Hence the nanofibers of NFBT functioned as a barrier, preventing the uncontrolled release of NFT, and the drug could only be released into the PBS when the outermost drug was dissolved. Thus, a sustained release of NFT was achieved. A prolonged release was also found in agar, the NFBT-NFT showed sustained inhibition of *E. coli* and *S. aureus* for 14 days (Fig. S4).

Fig. 2(E)–(G) show that the release behavior of NFBT-RB was significantly different. In the first 24 h, over 80% of RB was released, after which the release of the drug slowed and maintained a uniform delivery until day seven. This difference could also be observed in the SEM images of Fig. 2(H). On day three, the NFBT still maintained a layered structure, while few RB crystals were observed in the cross-sectional samples. The results suggested that, despite the high water-solubility of RB, the multiple barrier effects of NFBT could maintain a controlled release of the drug for 7 d.

3.3. Cytotoxicity

The cytocompatibility of NFBT was evaluated by co-culturing L929 cells with NFBT extracts and the cell viability was measured by the CCK-8 assay. At 24 h and 72 h after seeding, the cell viability of the NFBT group showed no statistical difference with a negative control group (Fig. 3(A)). The long fusiform shapes of the cells from the NFBT group (at 72 h) were also consistent with the absence of toxic responses such as cell detachment, lysis, and extensive vacuolization (Fig. 3(B)). These results suggested that NFBT was suitable for use in vivo.

3.4. In vivo experiments

3.4.1. Implantation and urine examination

The NFBT-CTL or NFBT-NFT loaded with NFT (150 mg) was implanted into the left ureter of pigs using a typical ureteroscopy procedure via the urinary tract. During implantation (Fig. 4(A)), the structure of the NFBT was maintained under the friction of the urethra and ureter and it was successfully anchored in the kidney and bladder. The content of NFT was then monitored in the urine. Fig. 4(B) shows that the concentration of NFT decreased rapidly between 4 h (28.7 ± 10.4 $\mu\text{g/mL}$) and 24 h (9.4 ± 2.3 $\mu\text{g/mL}$) after implantation, and then declined slowly thereafter to 1.6 ± 0.5 $\mu\text{g/mL}$ at day 28. Patients with urinary tract infections typically receive 50 mg doses of NFT via capsules administered orally every 6 h [35]. Approximately 30–50% of the administered dose is excreted via the urine in which concentrations of NFT range from 50 to 150 $\mu\text{g/mL}$ [36].

CFU counts were also determined in the urine collected from the implanted animals at regular intervals by the agar plate counting method. Fig. 4(C) and (D) show that the CFU count in the NFBT-CTL group was over $1 \times 10^5/\text{mL}$ at 4 h, and the values increased to $1\text{--}2 \times 10^6$ CFU/mL by day 28. In contrast, the NFBT-NFT group showed a significant bactericidal effect with no bacteria detected in the urine until day 28. The total amount of NFT administered by the NFBT was only 150 mg, which is about 2.68 wt% of the clinical oral dosage. Consequently, the concentration of drug measured in urine was much lower than amounts reported after oral administration, and it could be

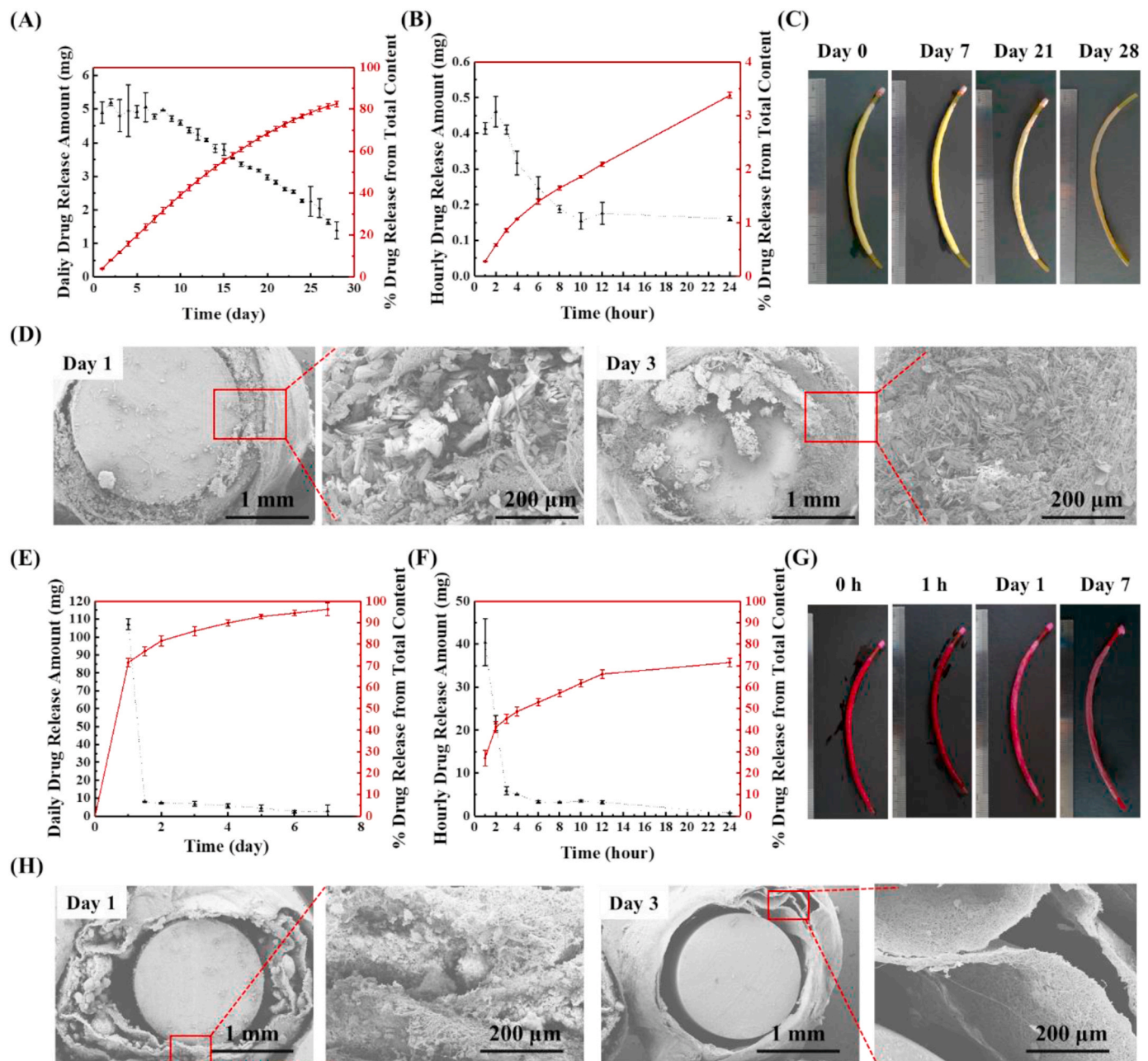


Fig. 2. Drug release characteristics of NFBT-NFT and NFBT-RB: (A) and (B) Long and short term drug release curves for NFBT-NFT; (C) images of NFBT-NFT before and after 7, 21, 28 d of in vitro drug release; (D) SEM images of NFBT-NFT on days one and three; (E) and (F) long and short term drug release curves for NFBT-RB; (G) images of NFBT-RB before and after 1 h, and 1 and 7 d of in vitro release; (H) SEM images of NFBT-RB on days one and three.

concluded that the in situ drug delivery system achieved much higher drug utilization.

3.4.2. Determination of biofilm and encrustation

The PU surface of the stents is hydrophobic and favors protein adsorption. This increases the receptor sites for bacterial adhesion-promoting the deposition of inorganic salts. Consequently, the formation of biofilm and encrustation are widely reported following the implantation of USs, and this contamination often contributes to US urinary infections. To evaluate this, the stent samples were removed 28 d after implantation and the extent of surface biofilm formation and encrustation was determined.

Fig. 5(A) shows the CFU counts obtained from the US part and NFBT of both implanted groups (NFBT-CTL and NFBT-NFT). The results showed that compared with the control, both components of the NFBT-

NFT reduced CFU by 99%. In both groups, adherent bacteria on the NFBT were significantly less than that on the stent part. This could be attributed to differences in surface topography between PU and NFBT, while NFBT-NFT provided a drug concentration gradient for bacterial inhibition.

SEM observation of the surface morphology of stents provided further insight. The large-scale image of NFBT-CTL in Fig. 5(C) revealed shell-like structures of around 1.6 μm thickness on the surface of the stent component. Within these structures, aggregated bacteria could be observed, indicating that the shell was a composite layer composed of organic matter, inorganic matter, and bacteria. Similar results were also observed on the NFBT component. The amount and type of inorganic deposits is an important characteristic of encrustation and five species of inorganic elements were detected in deposits on the NFBT-CTL group, contributing 3.68 and 2.31 wt% to the stent and NFBT components

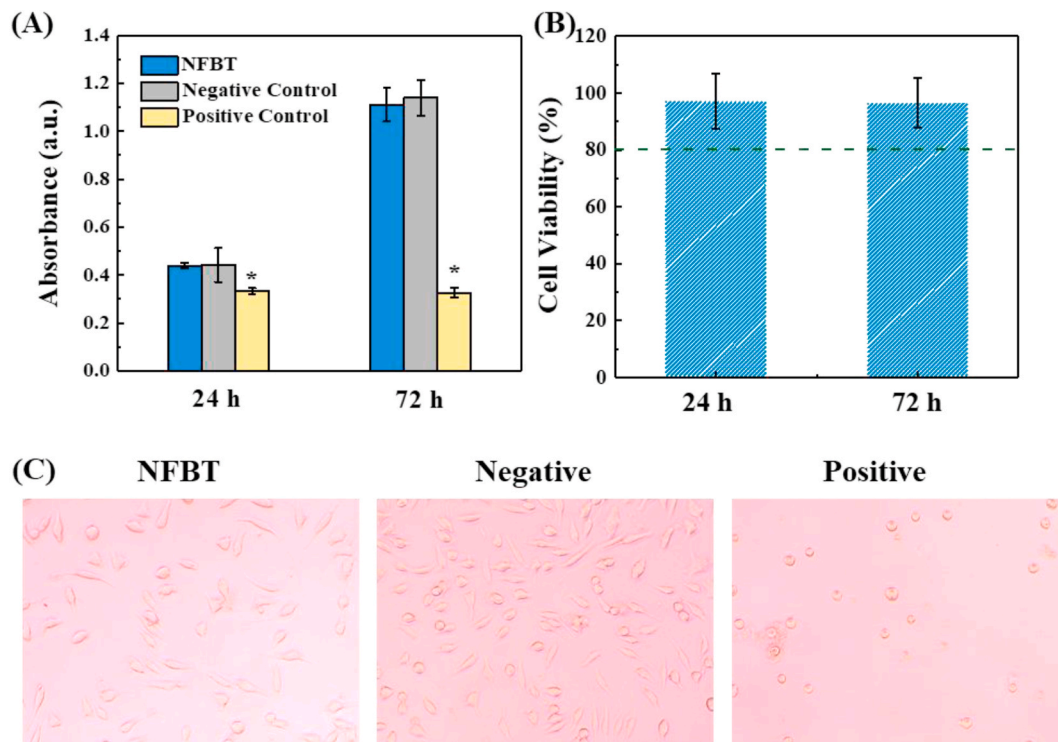


Fig. 3. Cytotoxicity results for NFBT. (A) UV absorbance from CCK-8 assay; (B) Cell viability of NFBT extraction; (C) L929 cell morphology after direct contact for 72 h.

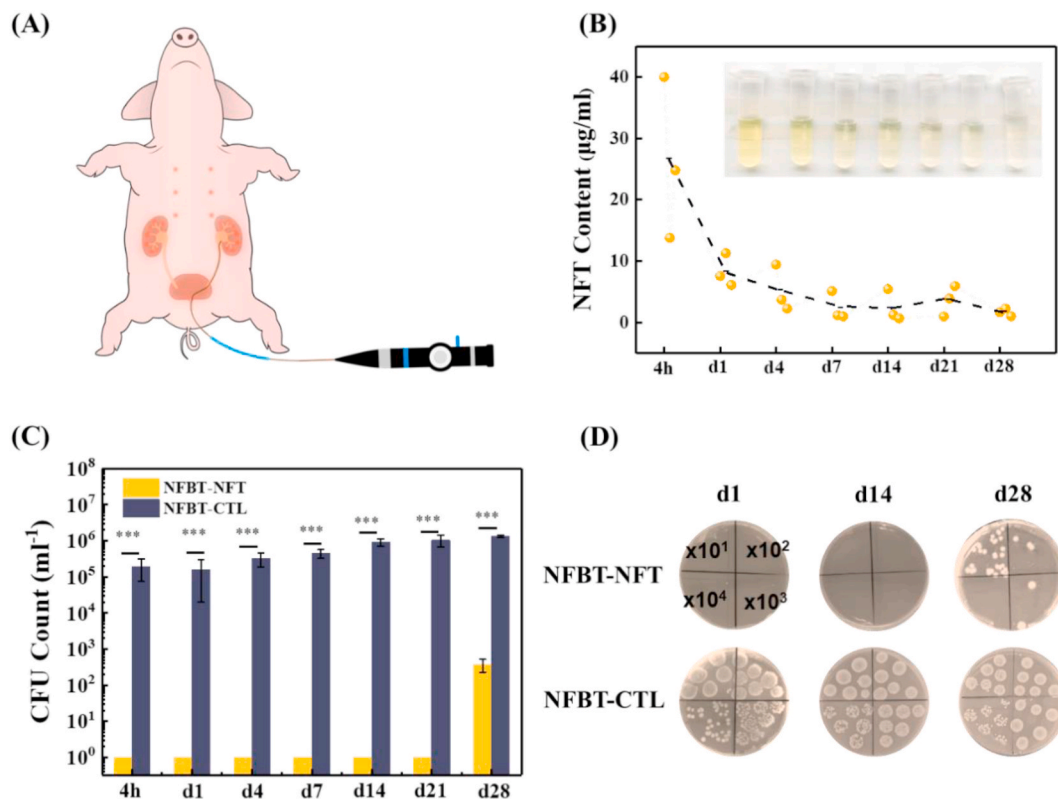


Fig. 4. Implantation and characterization of urine from the NFBT-NFT and NFBT-CTL groups: (A) Schematic diagram of the implantation method; (B) Detected NFT content in porcine urine; (C and D) Bacterial concentrations in urine measured by agar plate count. ****p* < 0.001.

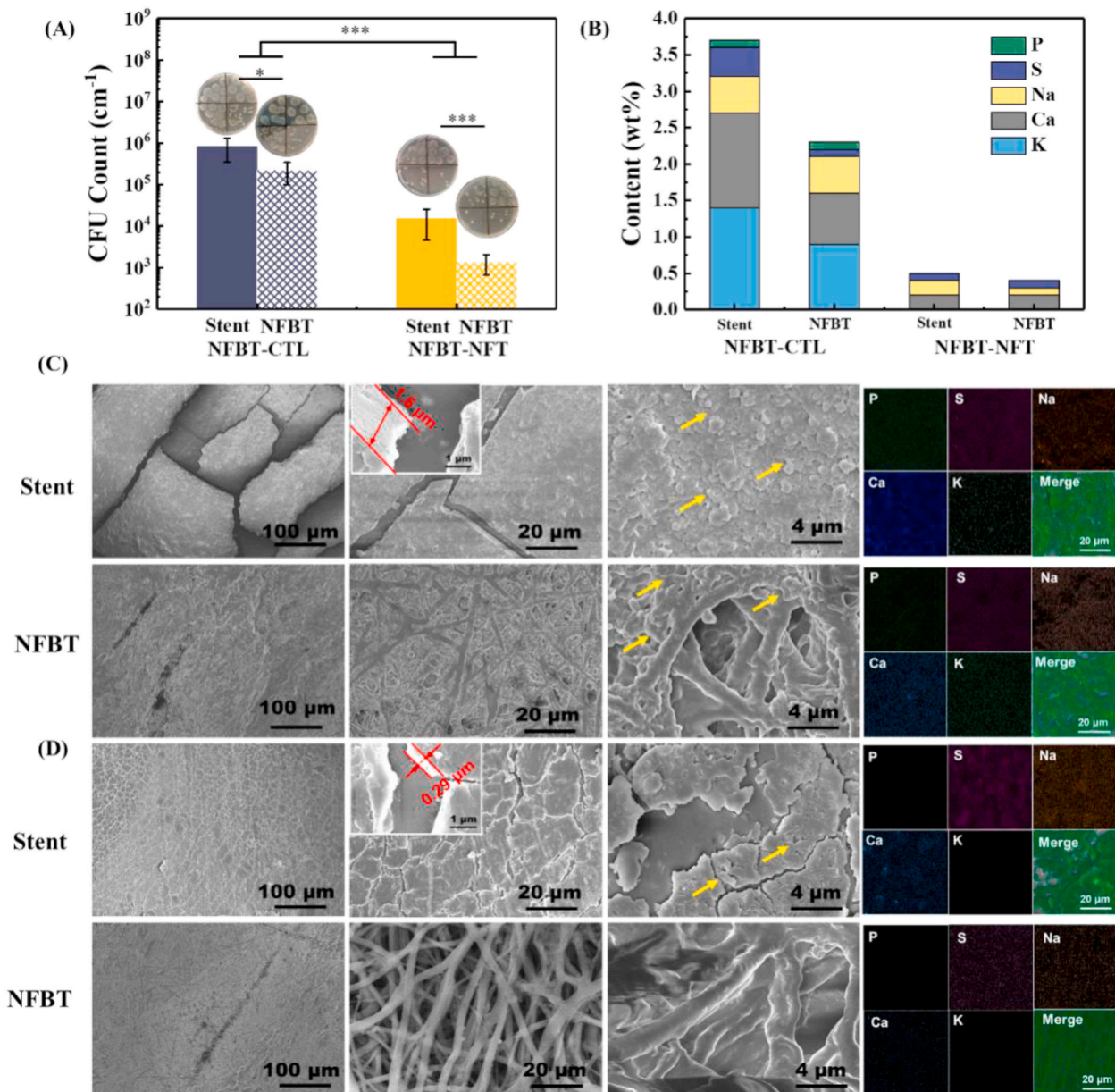


Fig. 5. Evaluation of in vivo biofilm formation and encrustation on stent components: (A) CFU bacterial counts; (B) surface element analysis; (C) SEM images and EDS analysis of NFBT-CTL; and (D) SEM images and EDS analysis of NFBT-NFT. * $p < 0.05$, ** $p < 0.01$, *** $p < 0.001$.

respectively (Fig. 5(B)). Three inorganic elements were found in the NFBT-NFT group, and the total amounts were <0.5 wt%, according to the in situ EDS scan of the demonstrated area of Fig. 5 (C). Although the shell-like structures were absent from the nanofibrous surface, a broad distribution of bacteria was observed. Biofilm formation and encrustation on the NFBT-NFT group were remarkably reduced (Fig. 5(D)). Although shell-like structures were also observed on the stent component, their thickness ($0.29 \mu\text{m}$) was 80% less than those of the NFBT-CTL group. As expected, the number of visible bacteria was also reduced, especially on the NFBT component. These results suggested that the release of NFT could significantly eliminate the adherence of bacteria, thereby preventing the formation of large-scale biofilm and encrustation on a stent. In addition, the NFBT component exhibited less bacterial adherence and deposition of inorganic matter due to its different surface properties.

3.4.3. Blood examination and histological analysis

To evaluate possible systemic toxicity induced by the NFBT or NFT,

key biomarkers of hepatic functions were monitored in blood samples from the implanted animals (Fig. 6). Compared with the initial values, the biomarkers of hepatic functions (i.e., ALT, ALT/AST, γ -GT, and TBA) showed no significant increases throughout the observation period. ALT and ALT/AST exhibited some fluctuations and the two groups showed statistical differences on days 7 and day 21. However, the values did not exceed the initial range and the two curves converged thereafter indicating no significant impact on the basic functions of the liver. These observations were also consistent with the histological examination of sections of the ureter (Fig. 7(C)). The liver cells exhibited normal morphology and no obvious necrosis, proliferation, or lymphocyte infiltration was observed.

Hematological analysis of the two groups also showed no obvious adverse effects on physiological indicators (i.e., WBC and LYM, Fig. 6). However, significantly higher WBC and LYM levels were found in the NFBT-CTL group on days 7 and 14 (compared with either initial values or the NFBT-NFT group) indicating a peri-implant infection induced by the invasion of bacteria. In contrast, the two indicators remained stable

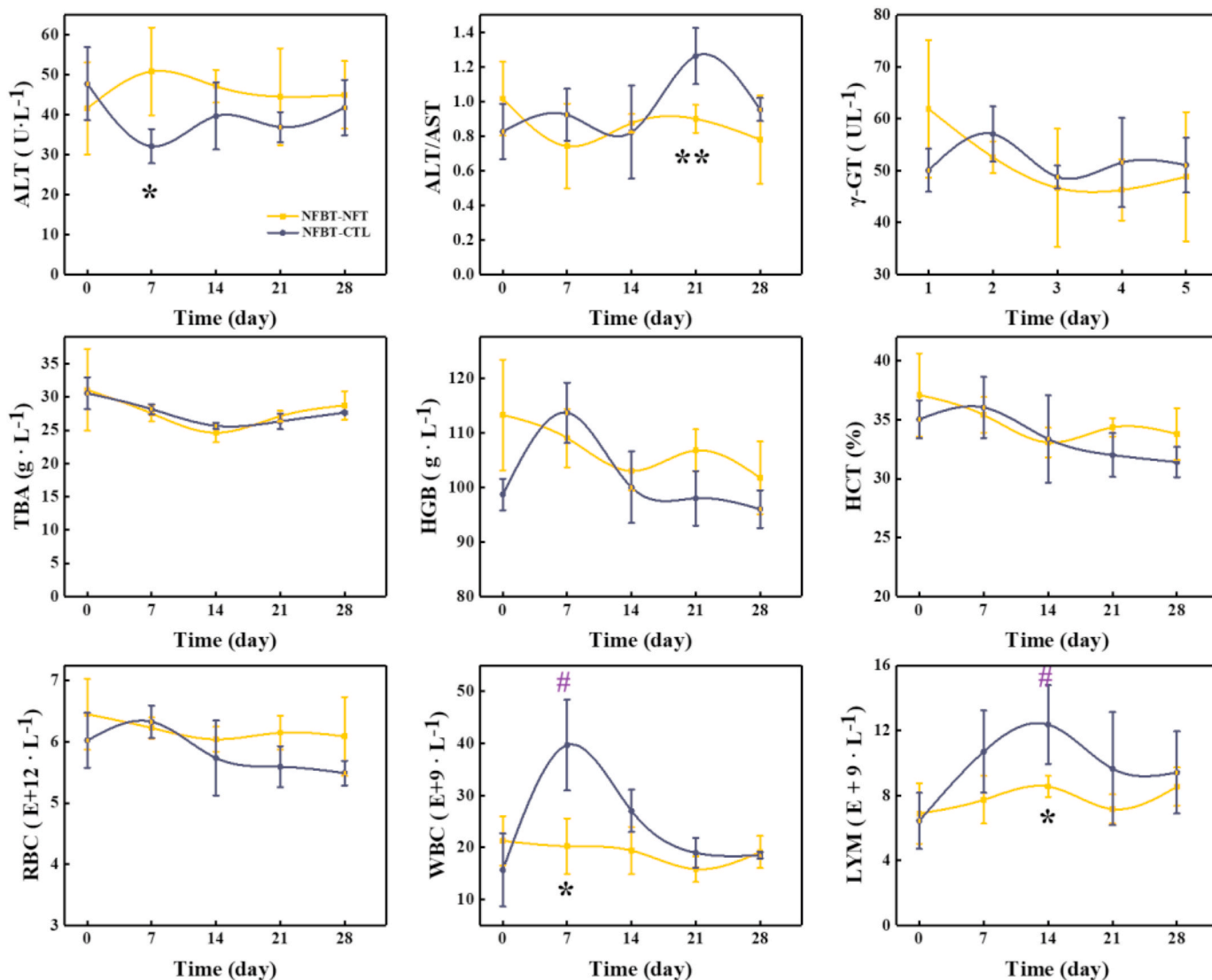


Fig. 6. Key indicators of systemic toxicity in the blood of test animals during the implantation period. Significant differences between NFBT-NFT and NFBT-CTL groups are marked with * ($p < 0.05$), ** ($p < 0.01$), and significant differences compared with day 0 are marked with # ($p < 0.05$), ## ($p < 0.01$).

in the NFBT-NFT group demonstrating that the sustained release of NFT could suppress the bacterial infection.

Further details of all urinary system tissues showing the different degrees of inflammation response are given in the images of Fig. 7. The ureters from both indwelled stents (NFBT-NFT and NFBT-CTL) were dilated and tortuous. Dilation and tortuosity are common in ureters with indwelled USs and they recover soon after stent removal. In the NFBT-NFT group, the left and right kidneys showed no significant morphological differences. However, the left kidney from the NFBT-CTL group was larger than the right kidney and the left renal pelvis was dilated, and its pelvic wall thickened. These pathological changes could be attributed to infectious inflammation (Fig. 7(A) and (B)). In addition, as highlighted in Fig. 7(A), after 28 days of implantation, the NFBT was still anchored on the upper part of the stent. Fig. 7(C) shows that the transitional epithelium of the left ureter exhibited some swelling in both groups (indicated on HE stained sections). This was more evident in the NFBT-CTL group where the epithelial tissue swelled to a thickness of 50.67 ± 11.5 μ m, and exfoliated vesicle tissue was observed internally. Examination of the CD 3 and CD 68 stained tissues revealed that the infiltration of T cells and macrophages in the NFBT-NFT group was lower than that in the NFBT-CTL group (Fig. 7(C)). Since the material of both groups in contact with this region of the left ureter was

polyurethane US, the immune rejection caused by the implant should be the same. The difference in inflammation response could be attributed to the diverse levels of infection, biofilm, and encrustation on the stent surface. The upper part of the left ureter that was directly in contact with NFBT was also stained and observed to investigate the histocompatibility of NFBT and NFT. Fig. 7(D and F) showed that the results from both groups were similar to that of the PUUS part, with epithelial tissue thicknesses of 35.6 ± 7.8 μ m in NFBT-NFT group and 53.3 ± 12.1 μ m in NFBT-CTL. This indicated that the histocompatibility of NFBT was like that of PUUS, and the locally high concentration NFT caused negligible additional irritation and damage to the tissue. The overall analysis on the thickness of epithelial tissue was shown in Fig. 7(G), the NFBT-NFT group was found to significantly suppress the inflammation degree, evidenced by the therapeutic efficiency of NFBT as a localized drug delivery system. In addition, compared with NFBT-NFT, the left kidney of NFBT-CTL showed swelling and dilation of the renal tubules. Epithelial tissue from the bladder of NFBT-CTL also showed a higher level of edema, ballooning degeneration, and inflammatory cell infiltration (Fig. 7(D and F)). The right kidneys and ureters were also examined, and a reduced level of inflammation was also observed in the NFBT-NFT group (Fig. 7(D)). Since these tissues did not contact directly with the implanted stents, a rejection response could be excluded and

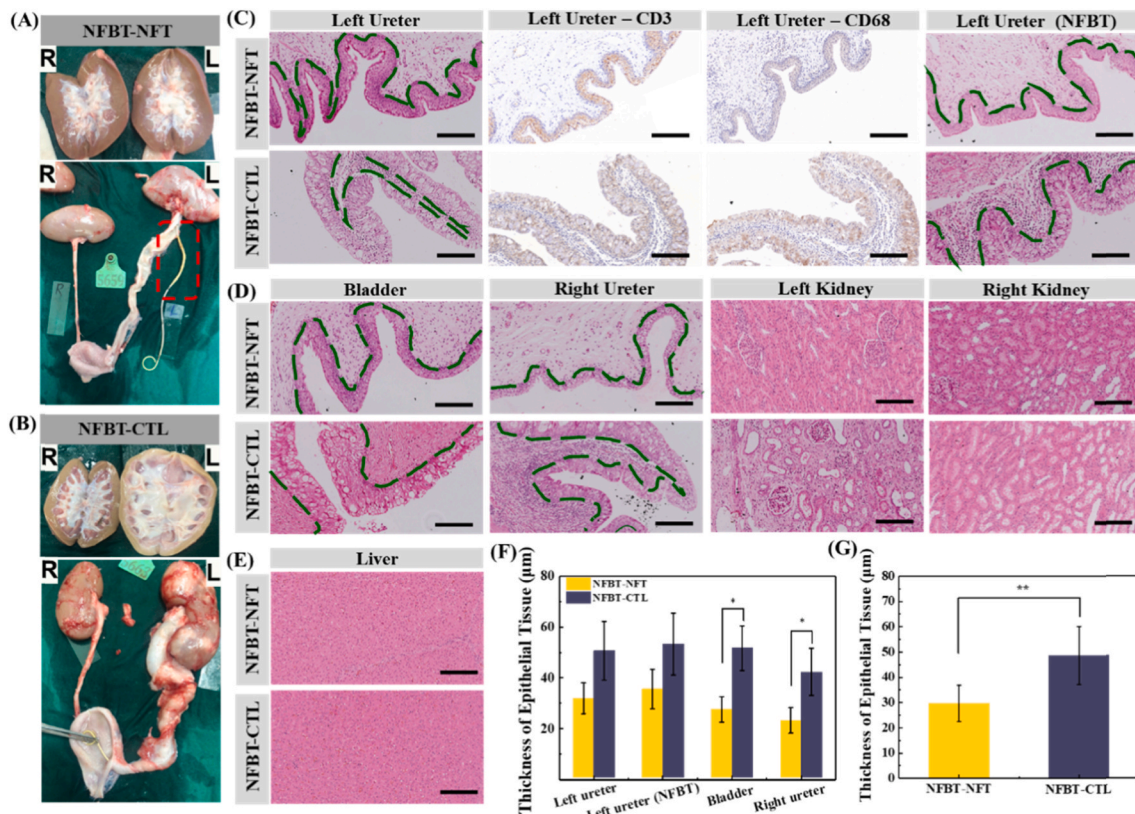


Fig. 7. Histological examination of the urinary system: (A) and (B) General observation of kidney and urinary tract; (B–E) representative HE, CD3 and CD68 stained sections at 28 d post-implantation (scale bars, 100 µm); (F) Statistical analysis on the thickness of epithelial tissue of ureter and bladder; (G) Significant analysis on the thickness of epithelial tissue in NFBT-NFT and NFBT-CTL groups.

the difference between the two groups should be due to inflammation induced by infectious agents. Therefore, the tissue stain results suggested that the sustained release of NFT could relieve infection of the whole urinary system by reducing the degree of bacterial invasion.

4. Conclusions

An ultrathin NFBT was prepared and evaluated as a self-adhesive drug delivery system for application to USs. Ultra-thin and elastic polycaprolactone (PCL) nanofiber membrane was prepared by electrospinning, and sodium hyaluronate was added to improve the hydrophilicity of the film. After loading with powdered drug, the bio tape could be rolled onto the commercial US under tension where it could maintain adhesion without additional measures. The release of drugs was prolonged by the multi-barrier structure of the NFBT. As a result, a sustained release of 7 d was obtained for the model hydrophilic drug RB, and a 28 d zero-order release for the hydrophobic drug NFT. In vivo experiments using a porcine ureteral tract infection model demonstrated that the NFBT had good biocompatibility, adhesive property, and sustained drug release behavior. Using a localized delivery of NFT to the stent environment, the level of urinary tract infection, biofilm formation, and encrustation were significantly improved. Compared with systemically administered agents, the amount of NFT dispensed was much lower.

Funding

The authors acknowledge the National Science Foundation for Young Scientists of China (No. 81902556), the Fundamental Research Funds for the Central Universities (No. 2232020G-01), the Fundamental Research Funds for the Central Universities and Graduate Student Innovation Fund of Donghua University (No. CUSF-DH-D-2021019),

China Scholarship Council (No. 202006630061), 111 Project (No. BP0719035).

Declaration of interest statement

None of the contributing authors have any conflict of interest, including specific financial interests or relationships and affiliations relevant to the subject matter or materials discussed in this article.

CRediT authorship contribution statement

Liheng Gao: Investigation, Methodology, Data curation, Writing – original draft. **Mingxi Xu:** Methodology, Visualization. **Wenshuo Zhao:** Data curation, Investigation. **Ting Zou:** Visualization. **Fujun Wang:** Data curation. **Jun Da:** Validation, Formal analysis. **Yiwei Wang:** Conceptualization, Methodology, Funding acquisition. **Lu Wang:** Supervision, Funding acquisition, Validation.

Appendix A. Supplementary data

Supplementary data to this article can be found online at <https://doi.org/10.1016/j.bioactmat.2022.03.025>.

References

- [1] M.P. Doogue, T.M. Polasek, Drug dosing in renal disease, *Clin. Biochem. Rev.* 32 (2) (2011) 69–73.
- [2] S. Desmedt, A. Spinewine, M. Jadoul, S. Henrard, D. Wouters, O. Dalleur, Impact of a clinical decision support system for drug dosage in patients with renal failure, *Int. J. Clin. Pharm.* 40 (5) (2018) 1225–1233.
- [3] G.M. Chertow, J. Lee, G.J. Kuperman, E. Burdick, J. Horsky, D.L. Seger, R. Lee, A. Mekala, J. Song, A.L. Komaroff, Guided medication dosing for inpatients with renal insufficiency, *JAMA, J. Am. Med. Assoc.* 286 (22) (2001) 2839–2844.

- [4] J.B. Wolinsky, Y.L. Colson, M.W. Grinstaff, Local drug delivery strategies for cancer treatment: gels, nanoparticles, polymeric films, rods, and wafers, *J. Contr. Release* 159 (1) (2012) 14–26.
- [5] Q. Chen, C. Wang, X.D. Zhang, G.J. Chen, Q.Y. Hu, H.J. Li, J.Q. Wang, D. Wen, Y. Q. Zhang, Y.F. Lu, G. Yang, C. Jiang, J. Wang, G. Dotti, Z. Gu, In situ sprayed bioresponsive immunotherapeutic gel for post-surgical cancer treatment, *Nat. Nanotechnol.* 14 (1) (2019) 89–91.
- [6] D. Svirskis, J. Travas-Sejdic, A. Rodgers, S. Garg, Electrochemically controlled drug delivery based on intrinsically conducting polymers, *J. Contr. Release* 146 (1) (2010) 6–15.
- [7] D. Campoccia, L. Montanaro, C.R. Arciola, A review of the biomaterials technologies for infection-resistant surfaces, *Biomaterials* 34 (34) (2013) 8533–8554.
- [8] C.R. Kim, E.B. Jang, S.H. Hong, Y.E. Yoon, B.K. Huh, S.N. Kim, M.J. Kim, H. S. Moon, Y.B. Choy, Indwelling urinary catheter assembled with lidocaine-loaded polymeric strand for local sustained alleviation of bladder discomfort, *Bioeng. Translat. Med.* 6 (2021), e10218, 2.
- [9] E. Necking, R. Levi, P. Ertzgaard, Complications of intrathecal drug delivery therapy (ITDD): a retrospective study of 231 implantations between 1999 and 2014, *Clin. Neurol. Neurosurg.* 205 (2021) 106630.
- [10] Y.Z. Wang, J.J. Li, I. Subramanian, G.D. do Vale, J. Chaudhary, A. Anwar, M. Wight-Carter, J.G. McDonald, W.C. Putnam, T. Qin, H.W. Zhang, I.R. Corbin, An implanted port-catheter system for repeated hepatic arterial infusion of low-density lipoprotein-docosahexaenoic acid nanoparticles in normal rats: a safety study, *Toxicol. Appl. Pharmacol.* 400 (2020) 115037.
- [11] K.E. Uhrich, S.M. Cannizzaro, R.S. Langer, K.M. Shakesheff, Polymeric systems for controlled drug release, *Chem. Rev.* 99 (11) (1999) 3181–3198.
- [12] A. Rafati, A. Boussahel, K.M. Shakesheff, A.G. Shard, C.J. Roberts, X. Chen, D. J. Scurr, S. Rigby-Singleton, P. Whiteside, M.R. Alexander, M.C. Davies, Chemical and spatial analysis of protein loaded PLGA microspheres for drug delivery applications, *J. Contr. Release* 162 (2) (2012) 321–329.
- [13] N. Abbasi, M. Navi, J.K. Nunes, S.S.H. Tsai, Controlled generation of spiky microparticles by ionic cross-linking within an aqueous two-phase system, *Soft Matter* 15 (16) (2019) 3301–3306.
- [14] J.Y. Li, D.J. Mooney, Designing hydrogels for controlled drug delivery, *Nat. Rev. Mater.* 1 (12) (2016) 1–17.
- [15] X. Zhao, B.L. Guo, H. Wu, Y.P. Liang, P.X. Ma, Injectable antibacterial conductive nanocomposite cryogels with rapid shape recovery for noncompressible hemorrhage and wound healing, *Nat. Commun.* 9 (2018) 1–17.
- [16] J.R. Lakkakula, P. Gujarathi, P. Pansare, S. Tripathi, A comprehensive review on alginate-based delivery systems for the delivery of chemotherapeutic agent: Doxorubicin, *Carbohydr. Polym.* 259 (2021) 117696.
- [17] M.A. Raza, Y.M. Lim, S.W. Lee, K.K. Seralathan, S.H. Park, Synthesis and characterization of hydrogels based on carboxymethyl chitosan and poly (vinylpyrrolidone): blends prepared by electron beam irradiation having anticancer efficacy, and applications as drug carrier for controlled release of drug, *Carbohydr. Polym.* 258 (2021) 117718.
- [18] X. Qin, Y. Xu, X. Zhou, T. Gong, Z.-R. Zhang, Y. Fu, An injectable micelle-hydrogel hybrid for localized and prolonged drug delivery in the management of renal fibrosis, *Acta Pharm. Sin. B* 11 (3) (2021) 835–847.
- [19] D.Y. Gu, A.J. O'Connor, G.G.H. Qiao, K. Ladewig, Hydrogels with smart systems for delivery of hydrophobic drugs, *Expert Opin. Drug Deliv.* 14 (7) (2017) 879–895.
- [20] B. Marco-Dufort, J. Willi, F. Vielba-Gomez, F. Gatti, M.W. Tibbitt, Environment controls biomolecule release from dynamic covalent hydrogels, *Biomacromolecules* 22 (1) (2021) 146–157.
- [21] E.D. Freitas, V.M.S. Freitas, P.C.P. Rosa, M.G.C. da Silva, M.G.A. Vieira, Development and evaluation of naproxen-loaded sericin/alginate beads for delayed and extended drug release using different covalent crosslinking agents, *Mater. Sci. Eng. C* 118 (2021) 111412.
- [22] L.L. Cai, S. Liu, J.W. Guo, Y.G. Jia, Polypeptide-based self-healing hydrogels: design and biomedical applications, *Acta Biomater.* 113 (2020) 84–100.
- [23] R. Olmos-Juste, B. Alonso-Lerma, R. Perez-Jimenez, N. Gabilondo, A. Eceiza, 3D printed alginate-cellulose nanofibers based patches for local curcumin administration, *Carbohydr. Polym.* 264 (2021) 118026.
- [24] S. Bose, N. Sarkar, D. Banerjee, Natural medicine delivery from biomedical devices to treat bone disorders: a review, *Acta Biomater.* 126 (2021) 63–91.
- [25] A. Melocchi, M. Ubaldi, A. Maroni, A. Foppoli, L. Palugan, L. Zema, A. Gazzaniga, 3D printing by fused deposition modeling of single- and multi-compartment hollow systems for oral delivery - a review, *Int. J. Pharm.* 579 (2020) 119155.
- [26] J.Y. Won, J. Kim, G. Gao, J. Kim, J. Jang, Y.H. Park, D.W. Cho, 3D printing of drug-loaded multi-shell rods for local delivery of bevacizumab and dexamethasone: a synergetic therapy for retinal vascular diseases, *Acta Biomater.* 116 (2020) 174–185.
- [27] J.C. Flores-Arriaga, D. Chavarria-Bolanos, A.d.J. Pozos-Guillen, V.A. Escobar-Barrios, B.I. Cerda-Cristerna, Synthesis of a PVA drug delivery system for controlled release of a Tramadol-Dexketoprofen combination, *J. Mater. Sci. Materials in medicine* 32 (5) (2021) 56, 56.
- [28] O.S. Kwon, J. Jang, J. Bae, A review of fabrication methods and applications of novel tailored microcapsules, *Curr. Org. Chem.* 17 (1) (2013) 3–13.
- [29] C.K. Wong, X.L. Qiang, A.H.E. Muller, A.H. Groschel, Self-Assembly of block copolymers into internally ordered microparticles, *Prog. Polym. Sci.* 102 (2020) 101211.
- [30] S. De Koker, R. Hoogenboom, B.G. De Geest, Polymeric multilayer capsules for drug delivery, *Chem. Soc. Rev.* 41 (7) (2012) 2867–2884.
- [31] X.T. Liu, Y.M. Liu, J.T. Du, X.R. Li, J.Y. Yu, B. Ding, Breathable, stretchable and adhesive nanofibrous hydrogels as wound dressing materials, *Engineered Regenerat.* 2 (2021) 63–69.
- [32] Y. Mao, M. Chen, R. Guidoin, Y. Li, F. Wang, G. Brochu, Z. Zhang, L. Wang, Potential of a facile sandwiched electrospun scaffold loaded with ibuprofen as an anti-adhesion barrier, *Mater. Sci. Eng. C* 118 (2021) 111451.
- [33] P. Wang, Y. Li, C. Zhang, F. Feng, H. Zhang, Sequential electrospinning of multilayer ethylcellulose/gelatin/ethylcellulose nanofibrous film for sustained release of curcumin, *Food Chem.* 308 (2020) 125599.
- [34] T. Malachowski, A. Hassel, Engineering nanoparticles to overcome immunological barriers for enhanced drug delivery, *Engineered Regenerat.* 1 (2020) 35–50.
- [35] Nitrofurantoin, Mechanism of action and implications for resistance development in common uropathogens, *J. Antimicrob. Chemother.* 33 (suppl A) (1994) 23–30.
- [36] M.I. Tasbakan, H. Pullukcu, O.R. Sipahi, T. Yamazhan, S. Ulusoy, Nitrofurantoin in the treatment of extended-spectrum β -lactamase-producing *Escherichia coli*-related lower urinary tract infection, *Int. J. Antimicrob. Agents* 40 (6) (2012) 554–556.